ACS OMEGA

Open Access

http://pubs.acs.org/journal/acsodf

Article

CO_2 Geostorage and Enhanced Oil Recovery: Challenges in Controlling Foam/Emulsion Generation and Propagation

Alexandra Klimenko,* Leyu Cui, Lei Ding, and Maurice Bourrel

Cite This: *ACS Omega* 2024, 9, 37094−37104

Read Online

ACCESS | Metrics & More | Article Recommendations | Supporting Information

ABSTRACT: CO_2 injection in subterranean reservoirs for storage, oil recovery, or both is challenging because of its very high mobility. Using a CO_2 foam or emulsion is a way to remedy this problem by increasing CO_2's apparent viscosity. However, the generation of the foam and its propagation in porous media present several issues that have to be overcome for this process to be economically realistic in practice. For example, it may take time, i.e., a number of pore volumes to be injected, before the foam is created. It is the objective of this Article to investigate these issues thoroughly and to identify the mechanisms underlying them by looking at the effects of various parameters. It is found that surfactant adsorption on the surface of the rock is an important factor involved in the delay of foam formation, but this may not explain all of the results. The nature and morphology of the porous medium may be, in some cases, the dominant factors for foam generation and propagation. From an understanding of the origin of the encountered problem, relevant mitigation strategies are envisioned and evaluated. It is found, for example, that when appropriately formulated and injected with the proper process, foam or emulsion generation is strongly accelerated, which very significantly shortens the delay for achieving CO_2 storage.

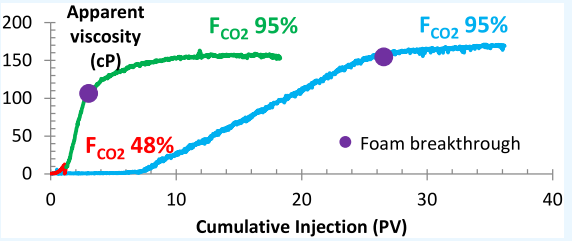

1. INTRODUCTION

CO_2 injection in subterranean reservoirs was initially developed for enhanced oil recovery (EOR) in depleted oil-bearing reservoirs.[1] Since then, with the awareness of climate breakdown, CO_2 EOR has appeared as an opportunity to sequestrate CO_2 underground while producing oil with a lower CO_2 emission footprint.[2−6] Besides, it has been recognized that saline aquifers offer also high storage potential,[7−10] possibly combined with geothermal heat extraction.[11]

In all of these situations, CO_2 has to displace residing water and, in some cases, some oil. Since CO_2 has a low viscosity, displacement is not piston-like, and in certain cases unstable viscous fingering may develop, yielding early breakthrough. Thus, reducing CO_2 mobility is highly attractive to stabilize the displacement front and increase the CO_2 storage capacity for a given reservoir. The potential advantages of foam for CO_2 storage and related challenges are discussed at length in the work by Rossen et al.[12]

A number of methods have been proposed for that purpose, including using additives in CO_2 to increase its viscosity or surfactants to create foams.[13] Depending on the relative permeability curves, the presence of oil, and the viscosity of the residing and injected fluids, it may be necessary to drastically reduce the mobility of CO_2 to displace the residing fluid. As an example, in experiences without oil or at residual oil saturation on a limestone core (Figure 1) without surfactant, we have estimated that the maximum apparent viscosity that needs to be overcome in the CO_2/water displacement front may vary from 0.6 to ∼5 cP. Since in this example the CO_2 viscosity is only 0.0273 cP, the mobility of CO_2 must be reduced by a factor of 22−183 to achieve piston-like displacement.

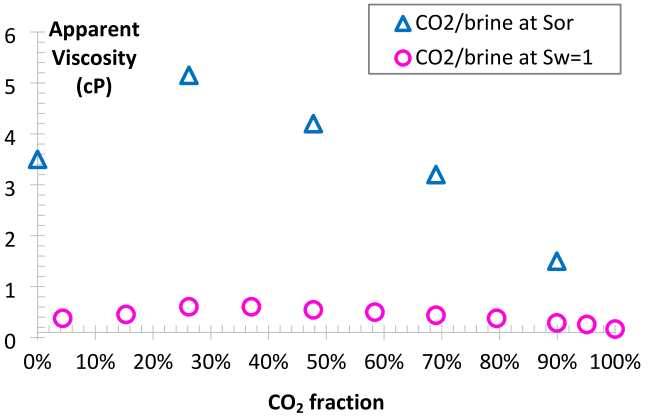

Figure 1. Apparent viscosity during brine/CO_2 coinjection on Estaillades at 4 ft/d in the absence (pink points) and in the presence (blue points) of the residual oil. Conditions: 110 °C, 150 barg.

Received: April 30, 2024
Revised: August 6, 2024
Accepted: August 8, 2024
Published: August 20, 2024

Such a reduction is possible if the CO_2 is injected in the form of a CO_2 foam, which forms between the brine and CO_2 thanks to a CO_2-philic surfactant. Clearly, the foam must be as CO_2-rich as possible while maintaining a high apparent viscosity to ensure the low mobility of the CO_2-rich phase. Recently, Li et al.[14] showed that, with CO_2 foam injection, the gas saturation increased from ∼21% (100% CO_2 injection) to ∼84% (85% CO_2-rich foam injection) after ∼10 PV of injection, therefore improving the CO_2 storage capacity. The best-performing foam also had the highest apparent viscosity, as derived from the measured pressure gradient, underlining the importance of good mobility control for CO_2 storage.

In this Article, we first record, from an application standpoint, several issues often encountered in the formation and propagation of the foam in porous media. We then present results obtained on quartz sandpacks of high permeability on the one side and on limestone cores of low permeability on the other side when varying various parameters. Afterward, we discuss the possible mechanisms underlying the observed phenomena. Finally, we propose some mitigation strategies depending on the identified issue.

2. EXPERIMENTAL CONDITIONS

Details are given in the Supporting Information. All experiments have been conducted at 150 barg and 110 °C unless specified. Under these conditions, CO_2 is in a supercritical state, and its density is 0.3031 g/cm^3, i.e., in between gas and liquid. We thus term the fluid either emulsion, foam, or emulsion/foam. All the indicated CO_2 fractions are volumetric and corrected for CO_2 solubility in brine (see Supporting Information).

The proprietary[15] surfactant R-CADA (reduced cocoalkyl dimethylpropane diamine) was used with a purity higher than 90%.[16] The brine salinity is 257.55 g/L total dissolved solids. Relative to other surfactants, this surfactant was shown to be capable of generating strong CO_2 foam with supercritical CO_2 at high temperatures with high-salinity brine. More details can be found in the work by Cui et al.,[16] and the molecular structure is presented in Figure 2.

R-CADA (N^1-coco alkyl-N^3, N^3-dimethylpropane-1,3-diamine), coco alkyl: C_{8-14}

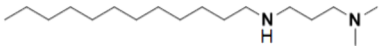

Figure 2. Molecular structure of R-CADA.

At these conditions, this surfactant is soluble in both CO_2 and saline brine (at pH ≤ 8). The measured partition coefficient is 1.82 ± 0.23 mole fraction in CO_2/mole fraction in brine (0.21 ± 0.07 g/L CO_2 per g/L brine) at 110 °C and 0.37 ± 0.13 mole fraction in CO_2 per mole fraction in brine (0.12 ± 0.04 g/L CO_2 per g/L brine) at 28 °C in 220 g/L NaCl brine and 150 barg (see the Supporting Information for more details). These values give minimum solubilities of ∼0.16 and 0.62 mg surfactant/g CO_2 at 28 and 110 °C, respectively.

The sandpack column was packed with quartz sand, giving 14 D permeability; limestone cores were from Indiana and Estaillades, with permeabilities around 330 and 130 mD, respectively.

To describe the mobility and strength of the CO_2 emulsion in different porous media, the measured pressure gradient ΔP is converted into apparent viscosity AV with the following equation based on the single-phase Darcy law:

$$\mathrm{AV} = k \cdot \frac{A}{q} \cdot \frac{\Delta P}{L}$$

where k is the absolute permeability, A is the core cross-section, q is the total volumetric injection rate, and L is the core length. All experiments are carried out by co-injecting CO_2 and brine containing R-CADA at a constant injection flow rate.

3. POTENTIAL CHALLENGES

A typical evolution of the apparent viscosity as a function of injected pore volumes is shown in Figure 3 together with the identification of its main features, which helps to display the requirements for successful foam/emulsion transport in the porous medium.

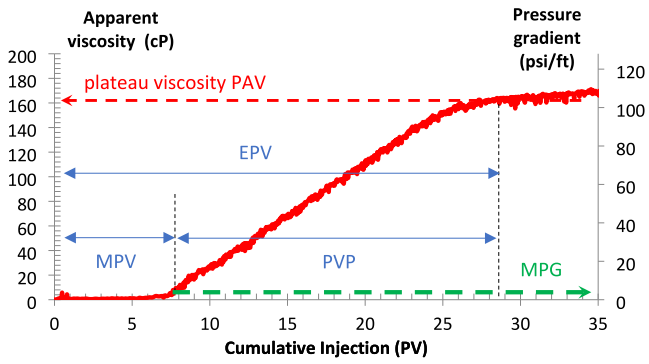

Figure 3. Definition of different typical characteristics of transient foam/emulsion transport in porous media initially saturated with brine. Example is based on an experiment on quartz sandpack, performed at 150 barg, 110 °C, and 0.95 CO_2 volume fraction (i.e., 95%); 0.2 wt % surfactant R-CADA in injected brine.

When co-injecting CO_2 and brine, with the surfactant injected into one of the phases (in this study, in the brine), it is common to observe a delay in emulsion/foam generation and development, the so-called minimum pore volume (MPV), which needs to be minimized to rapidly ensure the required mobility control.

At the minimum pore volume, the pressure gradient rises gradually until it sudden increases, indicating the formation of a strong foam/emulsion.[17] The MPV is generally attributed to the time required for the pressure to reach a minimum pressure gradient (MPG) that must be exceeded to start the formation of a strong foam/emulsion. Among the other parameters listed below, MPV is a strong function of surfactant adsorption.

MPG increases with the foam quality, i.e., the CO_2 volumetric fraction,[17−19] with decreasing surfactant concentration,[19] with increasing surface tension,[17,18] and with decreasing pore throat radius.[18] Due to the latter, the relationship of MPG with permeability k is complex for consolidated porous media but simpler for unconsolidated media where MPG scales with $1/k$.[17] As the interfacial tension with CO_2 is lower than that with N_2, it has been shown[20] that MPG is much lower for CO_2 emulsion/foam (<2 psi/ft) than for nitrogen foam.

Once the foam/emulsion starts to form, it propagates through the porous medium, which takes a certain amount of

https://doi.org/10.1021/acsomega.4c04137
ACS Omega 2024, 9, 37094−37104

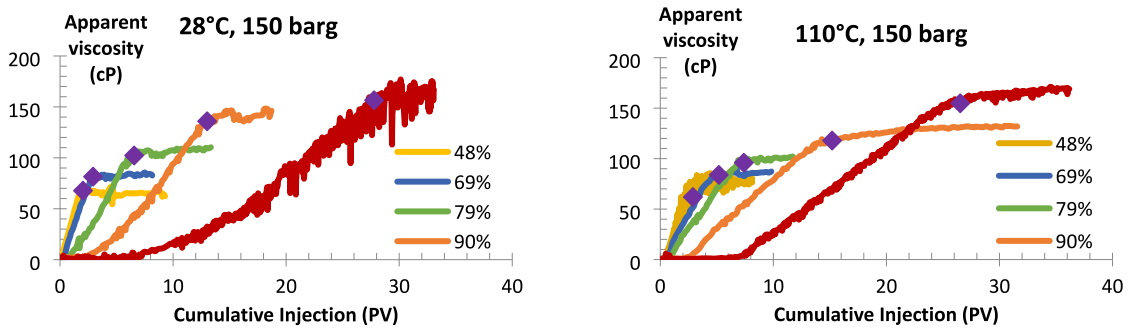

Figure 4. CO_2 emulsion generation at different CO_2 volume fractions coinjected at a Darcy velocity of 60 ft/d and 0.2 wt % R-CADA in brine in quartz sandpack (~14 D, 33% porosity). The sandpack is saturated initially with brine. Violet points define the emulsion breakthrough time.

time, defined here as the pore volume required for emulsion propagation (PVP). In constant-velocity experiments, when conditions are favorable for stable strong foam, this time is influenced by a number of parameters: the surfactant concentration,[21] which is subjected to adsorption and CO_2/brine partitioning; the dispersivity of the porous media; the injected foam quality; the core orientation;[22] the nature of the porous media; etc. During this time, the apparent viscosity continues to increase until it reaches a steady-state plateau.

The sum of MPV and PVP is the number of pore volumes required for the foam/emulsion to reach equilibrium (i.e., the plateau) and is defined here as EPV. The apparent viscosity at the plateau (PAV) is the steady-state emulsion/foam force for a given injected CO_2 volume fraction (F_{CO_2}). It is commonly observed that PAV exhibits a maximum upon variation of F_{CO_2}.

Besides, an important feature of foam/emulsion transport is the possible arrival of the foam/emulsion before EPV, which implies that the foam texture continues to evolve in the porous medium. This is the sign that foam forms at the outlet due to the capillary end effect and that, once formed, it generates backward against flow toward the inlet, resulting in an increase in apparent viscosity.[23−26]

Therefore, for successful injection, MPV, PVP, and MPG must be minimized while ensuring a high apparent viscosity PAV at the highest possible F_{CO_2}. The CO_2 volume fraction at the highest apparent viscosity is defined here as the transition quality $F^*_{CO_2}$. Finally, the effect of the presence of oil in the porous medium has to be taken into account.

4. RESULTS AND DISCUSSION

The investigation of the effect of various parameters on the features of the curve of apparent viscosity vs injected pore volumes (Figure 3) has been carried out on quartz sandpack (see the Supporting Information). The effect of the type and morphology of the porous medium is presented later.

4.1. Results. The apparent viscosity behavior at different CO_2 volume fractions F_{CO_2} at 28 and 110 °C is reported in Figure 4.

The steady-state apparent viscosity PAV increases with F_{CO_2} and is the highest at a foam quality of about 95%, thus satisfying one of the criteria for mobility control during CO_2 injection; additionally, it is not sensitive to temperature with the surfactant at hand, as shown in Figure 5.

The effect of the CO_2 volume fraction on MPV, PVP, and MPG is reported in Figure 6.

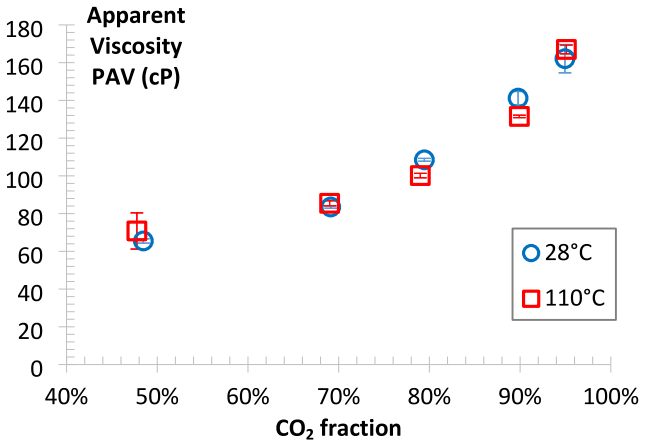

Figure 5. Steady-state apparent viscosity of the CO_2 emulsion generated in quartz sandpack (~14 D) at 60 ft/d and 0.2 wt % R-CADA in brine, 150 barg, and 110 °C.

As shown in Figure 6 (left side) and Figure 5, the steady-state emulsion strength increases with F_{CO_2} but is accompanied by an increase in MPV and PVP: more than 25 PV of injection is required to reach the steady-state condition at F_{CO_2} 95%.

Interestingly, MPG appears to be almost constant (1−2 psi/ft) with F_{CO_2} (Figure 6, right side), in contrast to the studies from Gauglitz at al.[17] and Yu et al.,[19] which predicted and showed an increase in MPG with F_{CO_2}. It is very likely that the interstitial gas velocity of 26−55 m/day in our experiments on sandpack was higher than the minimum velocity required for foam generation.[18] Therefore, the reported MPG is probably apparent, meaning that the observed delay (MPV) is related to other reasons and that the actual MPG is <1−2 psi/ft

As mentioned above, if oil is present in a target reservoir, even a small amount may be enough to increase the EPV and deteriorate the emulsion/foam strength: on quartz sandpacks (Figure 7, left side), the presence of residual oil considerably delayed CO_2 emulsion generation and, at 28 °C, decreased emulsion strength. This was confirmed by other experiments conducted on Estaillades limestone (Figure 7, right side), where 6% of oil was sufficient to hinder emulsion generation even after ~25 PV of emulsion injection. The negative impact of oil on CO_2 foam/emulsion generation and propagation is known under both immiscible and miscible conditions.[27−32] Therefore, the impact of oil on emulsion/foam generation, propagation, and stability must also be considered if the CO_2 emulsion/foam is to be injected into an oil-bearing reservoir.

https://doi.org/10.1021/acsomega.4c04137
ACS Omega 2024, 9, 37094−37104

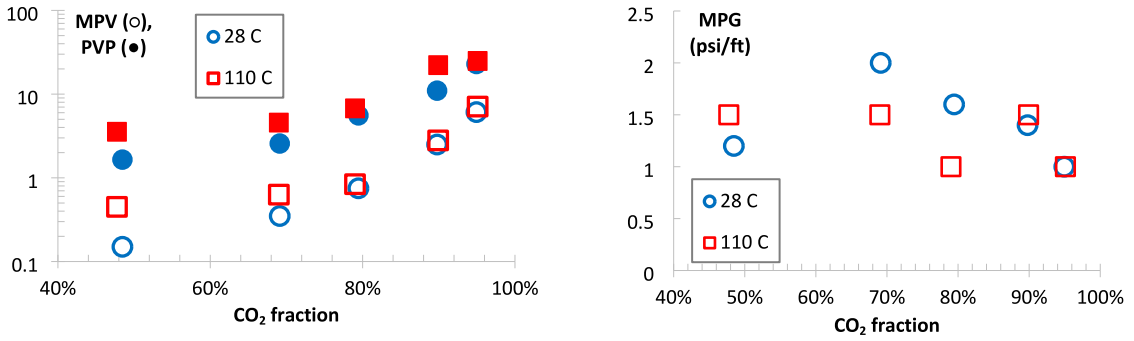

Figure 6. Characteristics of transient emulsion behavior during CO_2 emulsion injection in quartz sandpack (~14 D) at 60 ft/d and 0.2 wt % R-CADA in brine, 150 barg, and 110 °C.

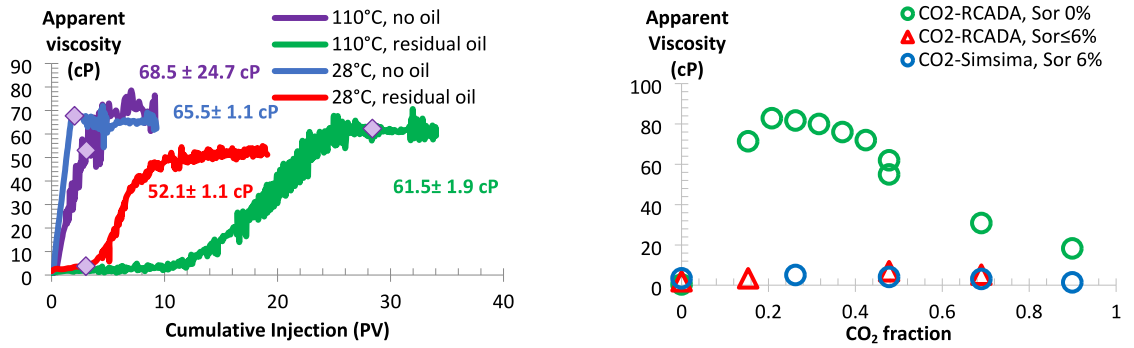

Figure 7. Oil impact during CO_2 emulsion injection (0.2 wt % R-CADA in the injected brine) under immiscible conditions. On the left: quartz sandpack, CO_2 fraction 48%, Darcy velocity 60 ft/d, 28 and 110 °C, 150 barg. On the right: quality scan on Estaillades limestone, 110 °C, 150 barg, 2 ft/d. Violet points define the emulsion breakthrough time.

In the following section, possible reasons for a delay in foam/emulsion generation and propagation are examined. Only oil-free conditions are discussed.

4.2. Discussion. The reasons for the delay of strong emulsion/foam generation and propagation must be elucidated in order to develop a strategy for accelerating foam/emulsion propagation for effective use of CO_2 injection. Hereafter, various possible reasons are examined. Only the strong foam/emulsion case of interest is discussed, as the propagation and generation of weak foams are out of the scope of this work.

4.2.1. Surfactant Adsorption. A necessary condition for foam and emulsion propagation is surfactant propagation, which can be compromised by adsorption.

The adsorption of a surfactant on a mineral is largely dependent on temperature, wettability, surface charge, pH, brine compositions, and salinity.[33,34] Presumably, the adsorption of the cationic surfactant (as amine surfactants at low pH) on carbonate minerals should be low at low pH since they are both positively charged.[35,36]

Static adsorption tests have generally been used to measure the adsorption of switchable amine surfactants on carbonate, and the pH was adjusted by pressurizing under 1−2 barg of CO_2.[37−39] However, the CO_2 solubility in brine at 2 barg is significantly lower than that at target high pressure (150 barg in the examples of this study). The brine composition and the extent of ion exchange may be largely different at different CO_2 pressures, which can impact the mineral surface charge.[40] More generally, the reliability of the static adsorption test is questionable since, first, normalization by the surface area must be performed to convert the data into the usual units of mg/g of rock and, second, the rock must be ground prior to the test, which can change the nature and even the charge of the surface[41] exposed to the surfactant solution.

Ideally, surfactant adsorption is more relevantly determined from dynamic measurements, i.e., by measuring the delay between the production profiles of the surfactant and a nonadsorbing tracer in a flooding experiment in a core of the porous medium under investigation. In the case of CO_2 injection at high pressure, as stated above, care must be taken with regard to the CO_2 solubility in water, and measurements at atmospheric pressure might not be relevant. A method has been developed in our laboratory to overcome this difficulty (patent pending,[42] see the Supporting Information). Applied on Estaillades limestone, it yields an adsorption of 0.19 ± 0.02 mg/g of rock or 0.42 ± 0.04 mg/m^2 of rock surface, the specific area having been determined by BET measurements.

However, this method is inconclusive in the case of the sandpack owing to its small pore volume and solid surface area. In the experiments on the sandpack, since the pressure gradient is assumed to be sufficient to overcome the MPG, the most obvious reason for the observed delay for foam/emulsion generation remains surfactant retention, likely essentially adsorption. This can be evaluated by calculating the mass of surfactant consumed before emulsion breakthrough, which corresponds to EPV, as follows:

$$m_{surf} = (PV_{bt}\cdot(1 - f_{CO_2}) - 1)\cdot C_s\cdot PV$$

where PV_{bt} is the number of pore volumes at which the emulsion arrives, PV is the pore volume and C_s is the surfactant concentration.

https://doi.org/10.1021/acsomega.4c04137
ACS Omega 2024, 9, 37094−37104

At 110 °C, the injected mass before steady state is established as almost constant (5.9 ± 0.8 mg, see Figure 8).

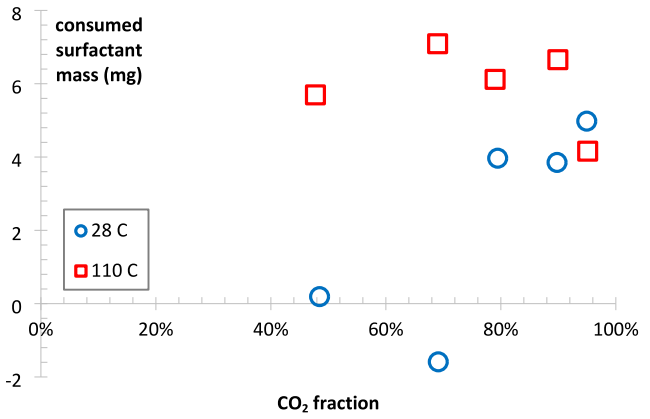

Figure 8. Injected surfactant mass "consumed" before emulsion arrival in the experiments on quartz sandpack.

At 28 °C and higher CO_2 fractions, the mass is also constant (4.3 ± 0.5 mg); the results at F_{CO_2} 48% and 69% are close to zero, and the experiments are worth repeating. In terms of adsorption, these values provide 0.12 ± 0.01 and 0.17 ± 0.02 mg/g of rock at 28 and 110 °C, respectively. The increase in estimated adsorption with temperature can probably be related to weaker interactions of the surfactant with brine at higher temperature.

The measured specific surface of the sand is 0.22 m^2/g, yielding adsorption values of 0.56 and 0.78 mg/m^2 at 28 and 110 °C, correspondingly. These values are higher than that measured on Estaillades limestone, which can be related to the difference in surface charges between quartz and calcite. A comparison with the adsorption of surfactants of comparable structure reported in the literature is provided in Table S3 of the Supporting Information.

To further establish the importance of surfactant adsorption in the transport process, an experiment was carried out on the same sandpack without restoration, i.e., co-injecting CO_2/brine with stepwise increasing fractions of CO_2. If adsorption is one cause of the delay, emulsion generation and propagation are expected to be rapid once adsorption is satisfied, since, as discussed before, the interstitial CO_2 velocity is sufficiently high to provide a pressure gradient higher than MPG. Indeed, as shown in Figure 9, less than 1 PV is required to generate the new emulsion, and only a few PV are required to reach steady-state conditions. Additionally, quality scans performed with and without restoration are in excellent accord (see Figure S4 in the Supporting Information).

Surfactant partitioning into CO_2, which significantly depletes the brine, especially at high CO_2 fractions, is a phenomenon that also possibly affects its transport in the porous medium. Interestingly, in our experiments, it does not lead to a decrease in emulsion strength at steady state, nor does it prevent emulsion/foam generation. At F_{CO_2} 95%, the estimated concentration in brine, obtained from the measured the partitioning coefficient $K_{CO_2/w}$ = 1.82 ± 0.23 mole fraction in CO_2 per mole fraction in brine at 110 °C, is 0.042%, close to the critical micellar concentration (CMC) determined from surface tension measurements, i.e., 0.046 wt %.[43] Such a low concentration should be far below the critical surfactant concentration where the emulsion/foam strength decreases with decreasing concentration. In addition, Mannhardt and Svorstøl[44] showed that the lowest surfactant concentration at which foam is generated overlaps with the CMC region. Therefore, it may be hypothesized that the surfactant present in both phases plays a role in foam/emulsion flow, not only in the aqueous or CO_2 phase.

4.2.2. Effect of the Nature of the Porous Media. Besides the propagation of the surfactant, the foam/emulsion itself has to be generated and propagated.

Generation, through MPG, is inversely related to the pore throat radius and the distance between two moving lamellae.[18,17] Therefore, the morphology of the porous media is a paramount factor for foam generation.

Its impact on propagation, i.e., on PVP, is less clear. In different population-balance models, which try to reproduce foam generation and the transient regime of foam propagation, lamella creation and destruction rates as well as foam texture are tuned to provide gas resistance to the flow. Depending on the model, rates of generation and coalescence are the function of foam texture, gas velocity, surfactant concentration, capillary pressure, pore geometry, and matching coefficients.[45,46] Dependence on the gas velocity reflects the idea that limiting capillary pressure decreases with increasing gas velocity,[47] whereas in a recent experimental study the opposite trend was shown.[48] In any case, capillary pressure and limiting capillary pressure are related to the two characteristics of the porous

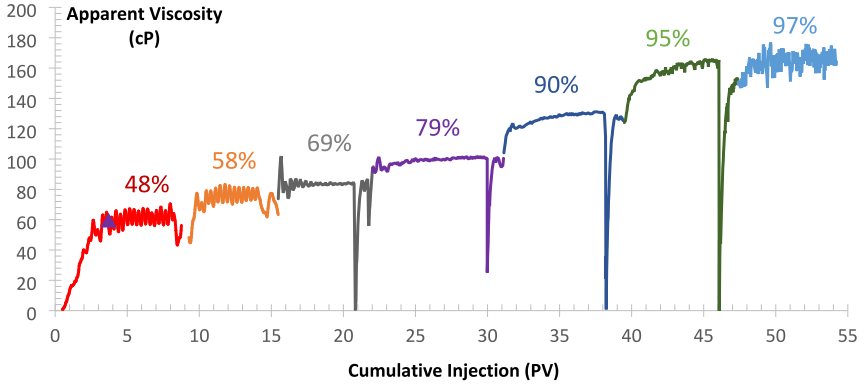

Figure 9. Flooding history of the coinjection of CO_2 and R-CADA solution at 0.2 wt % in brine in quartz sandpack at a superficial velocity of 60 ft/d, 110 °C, and 150 bar. % indicates the CO_2 volume fraction. The violet point defines the emulsion breakthrough time.

https://doi.org/10.1021/acsomega.4c04137
ACS Omega 2024, 9, 37094−37104

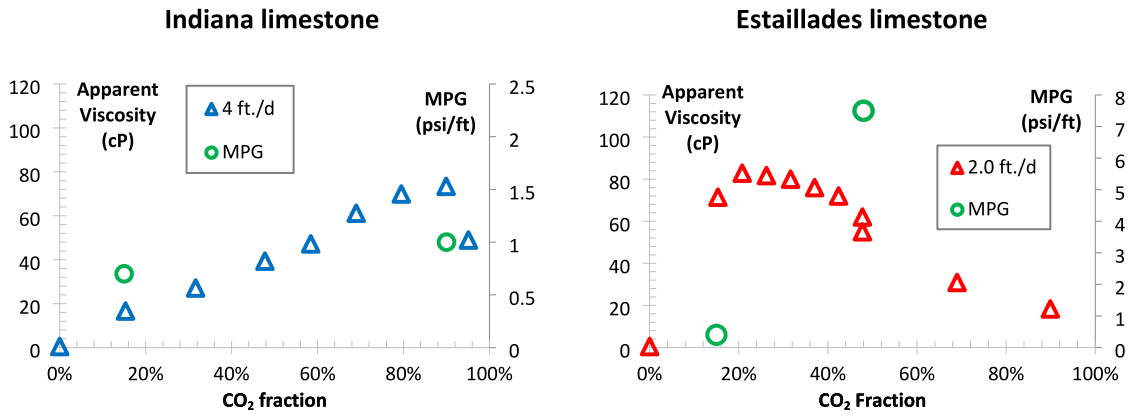

Figure 10. Quality scan and MPG in Estaillades (on the right) and Indiana (on the left) limestones. Conditions: 110 °C, 150 barg, 0.2 wt % R-CADA in brine. MPG on both limestones is measured at 4 ft/d.

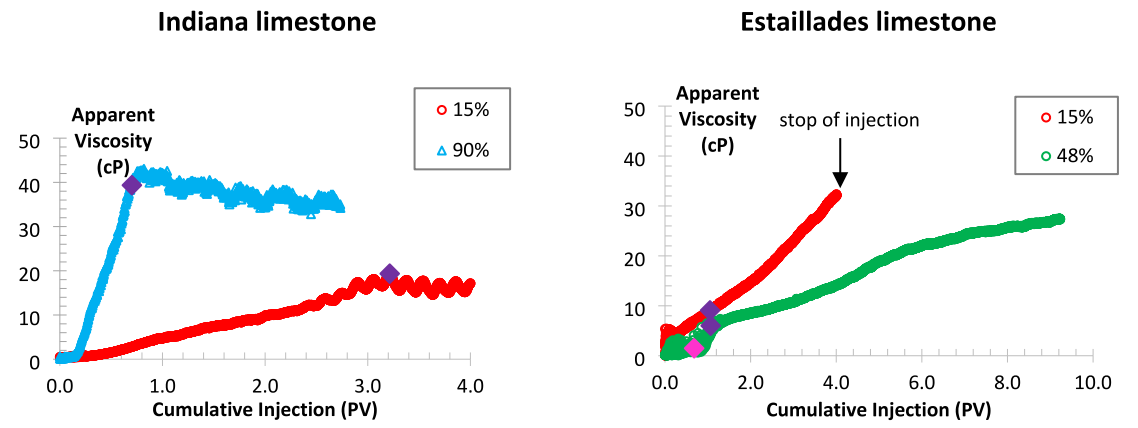

Figure 11. CO_2 emulsion generation after preflushing with a R-CADA solution at different CO_2 volume fractions on Estaillades (on the right) and Indiana limestone (on the left) at a Darcy velocity of 4 ft/d and 0.2 wt % R-CADA in brine. Violet points define the emulsion breakthrough time. Magenta points indicate CO_2 arrival.

media, i.e., wettability and pore throat diameter, which are expected to impact the transient behavior, i.e., the PVP value.

The effect of the rock type was investigated on limestone cores from two different origins: Estaillades and Indiana. To avoid being hampered by surfactant adsorption, quality scans in the coreflood experiments have been carried out without any restoration in between two successive injections, similar to Figure 9.

The results at steady-state conditions obtained on Estaillades (Figure 10, left side) and Indiana limestones (Figure 10, right side) are very different: $F^*_{CO_2}$ is near ∼20% and ∼90%, respectively, while in the quartz sandpack it is ≥95% (Figure 5). The low $F^*_{CO_2}$ value observed for Estaillades has already been mentioned by Ding et al.,[49] who reported $F^*_{CO_2}$ < 50% with nitrogen foam in the presence of oil. As yet, no explanation has been found for this unusual behavior, but it is probably related to the complex porous structure of this limestone.[50]

Both limestones have similar pore throat diameter distributions[51] and thus the notable difference in quality scans is surprising. This possibly underlines the importance of other petrophysical characteristics: Indiana limestone is more permeable and less porous than Estaillades.

Emulsion generation and propagation were studied for two F_{CO_2} values after a preflush with a surfactant solution to satisfy the adsorption at 15% and 48% on Estaillades and at 15% and 90% on Indiana limestone. The results are presented in Figure 11, and MPG is reported in Figure 10.

On Indiana limestone, MPVs are nonzero and close for both F_{CO_2} (∼0.2 PV); as for MPG, it increases slightly with F_{CO_2} from 0.7 to 0.9 psi/ft (Figure 10, left). Propagation is much faster for a stronger emulsion, i.e., for a higher CO_2 fraction.

On Estaillades, the behavior is very different: despite satisfied adsorption, MPV is more important at a higher CO_2 fraction (∼0.8 PV versus almost zero at F_{CO_2} 15%) and accompanied by a notable MPG increase from 0.4 to ∼7.5 psi/ft (Figure 10, right). The experiment at the low CO_2 fraction was interrupted before steady state was reached, but this continuous generation and propagation appears to be faster for a stronger emulsion as in Indiana limestone but at low CO_2 fraction. More importantly, emulsion breakthrough appears near 1 PV for both fractions tested and pressure continues to increase, indicating bubble refinement and emulsion texture evolution in the porous media, probably due to the presence of end effect on Estaillades: a strong emulsion is generated near the outlet and generates backward, progressively filling the core, as previously reported by Apaydin and Kovscek in 2001,[24] Nguyen at al. in 2003,[25] and Almajid et al. in 2019.[26] According to the studies cited, the weak, coarse emulsion first broke through, and then the emulsion strengthened as the front receded.

https://doi.org/10.1021/acsomega.4c04137
ACS Omega 2024, 9, 37094−37104

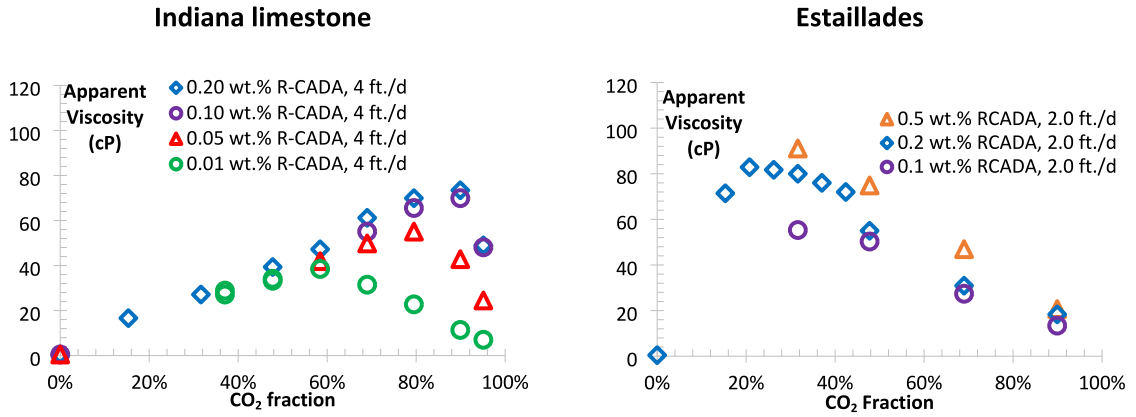

Figure 12. Quality scan in Estaillades (on the right) and Indiana limestone (on the left) for R-CADA concentrations in brine.

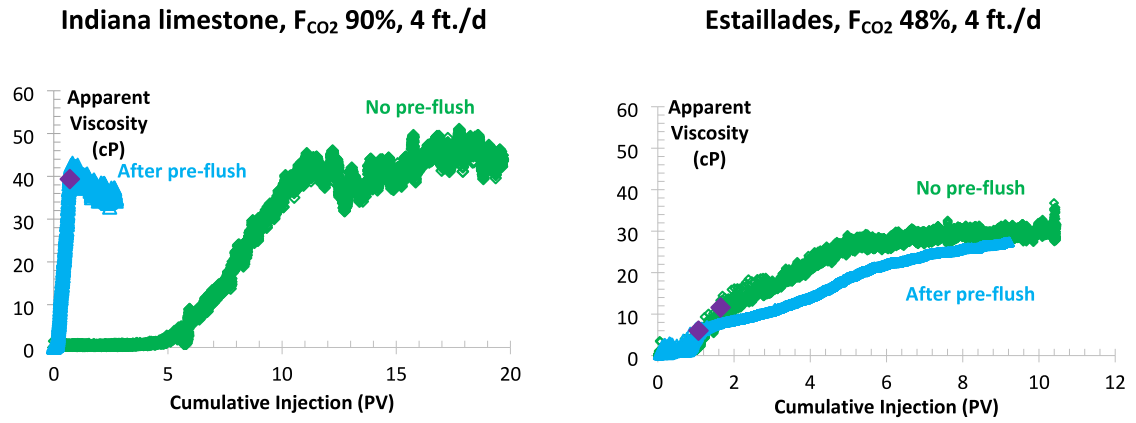

Figure 13. Impact of the preflush of R-CADA on transient emulsion behavior on Indiana limestone (on the left, F_{CO_2} 90%) and on Estaillades (on the right, F_{CO_2} 48%) at a Darcy velocity of 4 ft/d and 0.2 wt % R-CADA in brine. Violet points define the emulsion breakthrough time.

In light of this, the difference in MPG (Figure 10) between the two limestones may be related to different emulsion generation conditions.

In Indiana limestone, due to the low MPG, generation most likely occurs in the inlet, since the emulsion arrival coincides with the EPV. The observed MPV is therefore related to the time required to reach the MPG.

Generation on Estaillades appears to occur at the core outlet due to the end effect, meaning that reported MPGs are apparent since the pressure gradient in gas phase would be higher at the outlet due to higher capillary pressure gradient and water saturation gradient.[26] Therefore, the actual MPGs for strong emulsion generation should be even higher. At low CO_2 fractions, the apparent MPG is lower as well as the actual MPG because the end effect and capillary pressure gradient are less pronounced for a wetter foam, as experimentally confirmed by Almajid et al. in 2019.[26]

Analysis of the atypical quality scan with low $F^*_{CO_2}$ and the difficulties in generating strong emulsions at high CO_2 fractions despite the satisfied adsorption observed on Estaillades underline the important impact of the porous media on CO_2 emulsion behavior. It is therefore essential to perform experiments on a reservoir rock as soon as possible, since the choice of an analogue is very often based on similar porosity, permeability and, in the best case, pore throat distribution. However, this analogy may prove insufficient.

Indeed, particular attention must be paid to laboratory artifacts such as foam/emulsion generation due to the end effect. It must be pointed out, however, that this phenomenon can possibly also be produced in reservoirs by heterogeneities yielding discontinuities of capillary forces, as observed by Almajid et al. in 2019,[26] resulting in that case in a positive effect. However, taking this effect into account when designing the implementation of a CO_2 emulsion injection is challenging.

4.2.3. Surfactant Concentration Effect. For a given porous medium, there exists a surfactant concentration, so-called "critical", above which the emulsion/foam strength no longer depends on the concentration. Knowledge of this critical surfactant concentration is important for economic considerations.

It is actually different for the two carbonates studied in this work: for Estaillades it is ∼0.2 wt %, while for Indiana limestone it is ∼0.1 wt % R-CADA (Figure 12). These values are higher than the critical micelle concentration (CMC) determined for this surfactant (0.046 wt % by Chen et al. in 2023[43]), in agreement with Mannhardt and Svorstøl[44] conclusions according to which concentrations higher than the CMC are necessary to generate and propagate the foam. It should be noted that Mannhardt and Svorstøl also showed that, once formed and propagated, the foam could be maintained even at sub-CMC concentrations, which can help minimize surfactant requirements during field application.

Besides, it is interesting to note that the transition emulsion quality $F^*_{CO_2}$ decreases when the surfactant concentration is reduced from 0.1 to 0.01 wt % on Indiana limestone, going from 90% to 58%. This is related probably to less resistant

https://doi.org/10.1021/acsomega.4c04137
ACS Omega 2024, 9, 37094−37104

water films at low surfactant concentration causing film breakage, eventual bubble coalescence, and therefore a coarser foam/emulsion. This phenomenon is consistent with those reported in literature[52] and implies that an injection at high CO_2 fraction may be a compromise when performed at a surfactant concentration lower than the critical one.

The nature and morphology of the porous medium thus play a major role not only in the steady-state foam/emulsion force but also in foam/emulsion generation and propagation. While surfactant retention can be more or less easily overcome to improve foam/emulsion generation and propagation, the impact of porous media is more difficult to handle. Several mitigation strategies are proposed depending on the main cause of the issue.

4.2.4. Mitigation Strategies. Indeed, for CO_2 emulsion injection for EOR or CO_2 storage applications, the higher the CO_2 fraction is, the better. It is required that at this fraction the emulsion/foam has a high apparent viscosity to efficiently displace water and/or oil. As was shown, for a given surfactant, this requirement can be met (Figures 5 and 10, right) or not (Figure 10, left) depending on the porous media. Of course, efficient injection requires also rapid emulsion/foam generation and propagation, which depends on adsorption, emulsion quality, force, and the porous nature, as seen above.

If the adsorption is a key factor in the delay of foam/emulsion generation, then the injection of a slug with a higher surfactant concentration is expected to reduce this delay. This strategy was tested on Indiana and Estaillades limestones.

Preflush injection of 0.2 wt % R-CADA solution for several pore volumes did accelerate the emulsion generation when injecting F_{CO_2} 90% on Indiana limestone (Figure 13): MPV decreased from ∼5 PV to ∼0.2 PV, and PVP decreased from ∼6.3 to ∼0.6 PV with no impact on MPG. Therefore, adsorption has an impact on both MPV and PVP, as previously hypothesized. If the difference in EPV of ∼10.6 PV is attributed to the adsorption, this would give ∼0.17 mg/g of rock, a value similar to that measured on Estaillades.

Using the adsorption value measured on Estaillades (§ 4.2.1 above), ∼1.5 PV of emulsion injection at F_{CO_2} 48% would be required to satisfy adsorption. However, preflush on Estaillades in the experiments at F_{CO_2} 48% only impacts MPV and emulsion breakthrough time without impacting PVP: MPV decreases slightly from ∼1 to ∼0.8 PV, and emulsion breakthrough time decreases from ∼1.6 to ∼1.0 PV while remaining well before the steady-state plateau, again indicating the presence of an end effect and backward strong emulsion generation into the core. Consequently, the observed MPV is only apparent and should not be considered as relevant. As emulsion generation occurs at the outlet, attaining the steady state (i.e., PVP) reflects just backward emulsion generation toward the inlet, which explains the comparable values of EPV for both experiments.

Therefore, the generation of strong emulsion is much more difficult on Estaillades, especially at high CO_2 fractions, and adsorption, i.e., the surfactant dilution effect, may not be as important as the MPG effect.

At low CO_2 fractions, as discussed before, the MPG is likely lower, and the adsorption may play a role in that case in delaying emulsion generation. Indeed, when injected at F_{CO_2} 15%, the same strategy of preflush is more effective: after preflush, an emulsion is generated almost instantaneously (Figure 14), but this emulsion is coarse since pressure continues to increase after emulsion breakthrough, as noted before.

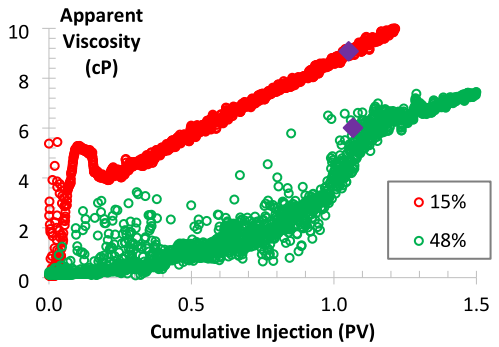

Figure 14. Zoomed-in view of the first 1.5 PV of Figure 11 (right). Violet points define the emulsion breakthrough time.

For cases such as Estaillades requiring high MPG for strong emulsion generation, a possible strategy may consist of a primary injection of a CO_2 emulsion requiring lower MPG (i.e., at lower CO_2 fraction) at sufficiently high flow rates to generate strong foam, and then the CO_2 fraction can be gradually increased to the desired value.

Alternatively, a combination of both strategies could be envisioned. This approach has been tested on quartz sandpack: the first injected slug was at F_{CO_2} 48%, for which fast emulsion generation was observed before. Moreover, to accelerate surfactant adsorption, this first slug contains 0.5 wt % R-CADA. Then, the slug of interest at F_{CO_2} 95% and 0.2 wt % R-CADA is injected, for which an important delay was previously observed with direct injection (Figure 6). The results are presented in Figure 15: for both temperatures tested, the use of a concentrated preflush, capable of rapidly generating an emulsion at low F_{CO_2}, considerably accelerates emulsion generation and propagation at higher CO_2 fractions.

Again, from a practical standpoint, given the importance of the nature of the reservoir rock as demonstrated above, it is advisable to use a reservoir core as early as possible starting from the first stage of the study, as the criteria for choosing the appropriate rock analogue are unclear. The strategy of injecting 2 slugs can be tested: either a preflush at high surfactant concentration or at low F_{CO_2}, if adsorption is found to be the reason for delayed foam/emulsion generation (as recommended by Mannhardt and Svorstøl in 2001[44]) or, if high MPG is the issue, the first slug at a CO_2 fraction for which fast generation of foam/emulsion was observed (generally, at low F_{CO_2}), followed by the target F_{CO_2}.

Regarding CO_2 storage implementation, ideally, the CO_2-containing surfactant should be injected into the target geological storage site. It is therefore important to assess whether an emulsion can be generated during the process to improve the sweep efficiency. Due to technical limitations in the laboratory, it was not possible to inject R-CADA dissolved in the CO_2 phase. To simulate this, CO_2 was injected into a surfactant-filled core of Indiana limestone. In doing so, we assume an instantaneous partition of the surfactant between the two phases.

A 3 PV slug at F_{CO_2} 5%, 0.2% R-CADA was first injected, followed by continuous injection of CO_2. Figure 16 illustrates the apparent viscosity and in situ CO_2 saturation during the R-

https://doi.org/10.1021/acsomega.4c04137
ACS Omega 2024, 9, 37094−37104

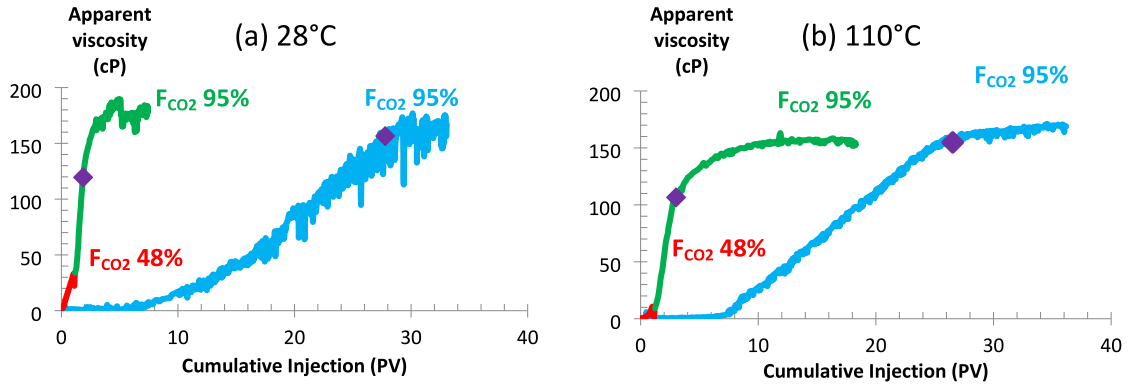

Figure 15. Impact of gradient injection (F_{CO_2} 48% to 95%) on emulsion generation on quartz sandpack. The slug at F_{CO_2} 48% contains 0.5 wt % R-CADA in brine, and the slug at F_{CO_2} 95% contains 0.2 wt % R-CADA in brine. Violet points define the emulsion breakthrough time.

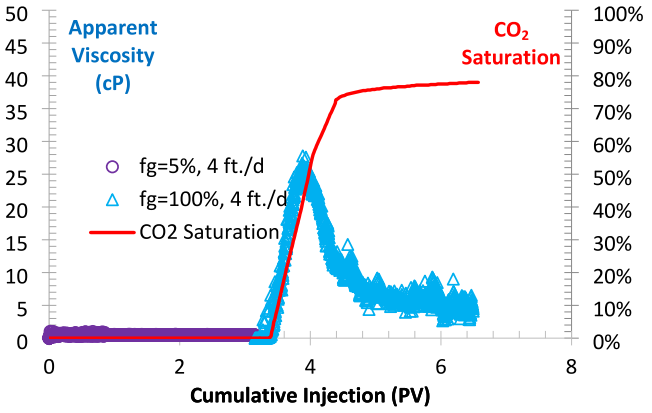

Figure 16. Emulsion apparent viscosity and CO_2 in situ saturation during R-CADA preflush and continuous CO_2 injection at 4 ft/d in Indiana limestone. Conditions: 110 °C, 150 barg, 0.2 wt % R-CADA in brine.

CADA preflush and subsequent continuous CO_2 injection. It is observed that upon the injection of pure CO_2 into the core, the emulsion is generated almost instantaneously. The peak of the apparent viscosity is around 27 cP, and the apparent viscosity is almost constant at 5 cP after 3 PV of CO_2 injection. CO_2 saturation was near 63% after the injection of ~3.5 PV of CO_2, while in the experiment without surfactant (not shown here) the injection of 9 PV of CO_2 was necessary to achieve this value.

5. CONCLUSIONS

It has been shown that the nature of the porous media and adsorption are key factors for the success of CO_2 emulsion/foam injection, controlling fast generation and propagation, as well as the high apparent viscosity at a high CO_2 fraction. As demonstrated, the mitigation strategy will vary according to which factor is most relevant to the desired objective.

The effects of various parameters (CO_2 volume fraction, temperature, and presence of oil) on transient and steady-state characteristics of foam/emulsion transport have been investigated on quartz sandpack of high permeability under conditions such that the pressure gradient was above the minimum pressure gradient. The steady-state emulsion strength increases with F_{CO_2}, but it is accompanied by an increase in the minimum pore volume and pore volume for emulsion propagation, which is a drawback to overcome.

Surfactant adsorption and the nature of porous media have been studied on two limestone materials coming from different sources. Despite having the same type of mineralogy, they yield very different behaviors: in one case, the foam/emulsion is formed at the inlet of the core with a delay of foam generation and propagation due to surfactant adsorption, while in the other case it is generated at the outlet of the core by the end effect, probably due to elevated minimum pressure gradient.

Two different mitigation strategies were thus proposed and evaluated to accelerate the achievement of the steady-state regime:

- If the consumption of surfactants by adsorption is the main reason for the delay, the injection of a concentrated preflush containing a sacrificial amount of surfactant can be a solution. It may be pertinent to inject this preflush at low F_{CO_2} to accelerate the satisfaction of adsorption.
- If the limitation is related to an insufficient pressure gradient to overcome the MPG, preinjecting a short slug at a CO_2 fraction for which MPG is lower enables the pressure gradient to be increased sufficiently to facilitate the foam/emulsion generation of the subsequent target F_{CO_2} slug.

In some situations, a slug at low F_{CO_2} may be the best choice for both strategies: a higher absolute amount of surfactant will satisfy adsorption faster than the target slug. Once adsorption is satisfied, it will provide some mobility control; finally, since generally the MPG of the wetter foam is lower, this simplifies the generation of the emulsion/foam of the target slug.

For applications in CO_2 storage, the CO_2 emulsion can substantially improve mobility control at the injected CO_2 front, provided it contains the surfactant capable of creating a strong emulsion.

This study also highlights the importance of porous media not only for steady-state conditions but also for the transition behavior of emulsion/foam (generation and propagation).

■ ASSOCIATED CONTENT

Supporting Information

The Supporting Information is available free of charge at https://pubs.acs.org/doi/10.1021/acsomega.4c04137.

Materials, experimental procedures, porous media properties, procedure for dynamic adsorption measurements, corresponding results, and interpretation (PDF)

https://doi.org/10.1021/acsomega.4c04137
ACS Omega 2024, 9, 37094−37104

AUTHOR INFORMATION

Corresponding Author

Alexandra Klimenko − *Pôle d'Etudes et de Recherches de Lacq, TotalEnergies S.E., 64170 Lacq, France; Physico-Chimie des Interfaces Complexes, Laboratoire Commun TotalEnergies/ESPCI, 64170 Lacq, France;* orcid.org/0000-0003-3810-385X; Email: alexandra.klimenko@totalenergies.com

Authors

Leyu Cui − *Pôle d'Etudes et de Recherches de Lacq, TotalEnergies S.E., 64170 Lacq, France; Physico-Chimie des Interfaces Complexes, Laboratoire Commun TotalEnergies/ESPCI, 64170 Lacq, France;* Present Address: Sinopec Shanghai Research Institute of Petrochemical Technology, 1658 Pudong Beilu, Shanghai 201208, China; orcid.org/0000-0003-2164-7586

Lei Ding − *Physico-Chimie des Interfaces Complexes, Laboratoire Commun TotalEnergies/ESPCI, 64170 Lacq, France;* Present Address: Aramco Asia, F 43, China World Tower, No. 1 Jian Guo Men Wai Avenue, Chaoyang District, Beijing 100004, P. R. China; orcid.org/0000-0002-0097-3000

Maurice Bourrel − *Physico-Chimie des Interfaces Complexes, Laboratoire Commun TotalEnergies/ESPCI, 64170 Lacq, France*

Complete contact information is available at: https://pubs.acs.org/10.1021/acsomega.4c04137

Notes

The authors declare no competing financial interest.

ACKNOWLEDGMENTS

TotalEnergies is gratefully acknowledged for allowing the publication of this work. We thank Mss. Géraldine Salabert and Michèle Joly for performing part of the experimental work.

REFERENCES

(1) Holm, L. W. Carbon dioxide solvent flooding for increased oil recovery. *Trans. AIME* **1959**, *216*, 225−231.

(2) Godec, M. L.; Kuuskraa, V. A.; Dipietro, P. Opportunities for using anthropogenic CO2 for Enhanced Oil Recovery and CO2 storage. *Energy Fuels* **2013**, *27* (8), 4183−4189.

(3) Ampomah, W.; Balch, R.; Cather, M.; Rose-Coss, D.; Dai, Z.; Heath, J.; Dewers, T.; Mozley, P. Evaluation of CO2 storage mechanisms in CO2 enhanced oil recovery sites: application to Morrow sandstone reservoir. *Energy Fuels* **2016**, *30* (10), 8545−8555.

(4) Kolster, C.; Masnadi, M. S.; Krevor, S.; Mac Dowell, N.; Brandt, A. R. CO2 -Enhanced Oil Recovery: a catalyst for gigatonne-scale carbon capture and storage deployment? *Energy Envir. Sci.* **2017**, *10* (12), 2594−2608.

(5) Iglauer, S.; Paluszny, A.; Rahman, T.; Zhang, Y.; Wülling, W.; Lebedev, M. Residual trapping of CO2 in an oil-filled, oil-wet sandstone core: results of three-phase pore-scale imaging. *Geophys. Res. Lett.* **2019**, *46* (20), 11146−11154.

(6) Sun, Q.; Ampomah, W.; Kutsienyo, E.; Appold, M.; Adu-Gyamfi, B.; Dai, Z.; Soltanian, M. R. Assess-ment of CO2 trapping mechanisms in partially depleted oil-bearing sands. *Fuel* **2020**, *278*, 118356.

(7) Garcia, S.; Kaminska, A.; Maroto-Valer, M. M. Underground carbon dioxide storage in saline formations. *Proc. Inst.Civil Eng.* **2010**, *163* (2), 77−88.

(8) Krevor, S.; Pini, R.; Zuo, L.; Benson, S. M. Relative permeabilities and trapping of CO2 and water in sandstone rocks at reservoir conditions. *Water Resour. Res.* **2012**, DOI: 10.1029/2011WR010859.

(9) Iglauer, S. CO2-water-rock wettability: variability, influencing factors, and implications for CO2 storage. *Acc. Chem. Res.* **2017**, *50* (5), 1134−1142.

(10) Ringrose, P. S.; Furre, A.-K.; Gilfillan, S. M. V.; Krevor, S.; Landro, M.; Leslie, R.; Meckel, T.; Nazarian, B.; Zahid, A. Storage of carbon dioxide in saline aquifers: Physico-chemical, key constraints, and scale-up potentials. *Ann. Rev. Chem. Biomol. Eng.* **2021**, *12*, 471−494.

(11) CO2-dissolved: successfully combining CO2 storage and geothermal extraction. *BRGM*, 2021. https://www.brgm.fr/en/reference-completed-project/co2-dissolved-successfully-combining-co2-storage-geothermal-heat

(12) Rossen, W. R.; Farajzadeh, R.; Hirasaki, G. J.; Amirmoshiri, M. Potential and Challenges of Foam-Assisted CO2 Sequestration. *Geoenergy Science and Engineering* **2024**, *239*, 212929.

(13) Massarweh, O.; Abushaikha, A. S. A review of recent developments in CO2 mobility control in enhanced oil recovery. *Petroleum* **2022**, *8* (3), 291−317.

(14) Li, S.; Wang, P.; Wang, Z.; Cheng, H.; Zhang, K. Strategy to enhance geological CO2 storage capacity in saline aquifer. *Geophys. Res. Lett.* **2023**, *50* (3), No. e2022GL101431.

(15) Cui, L.; Bourrel, M.; Dubos, F.; Klimenko, A. Surfactant for enhanced oil recovery. US 11254854 B2, 2022.

(16) Cui, L.; Dubos, F.; Bourrel, M. Novel alkyl-amine surfactants for CO2 emulsion assisted enhanced oil recovery. *Energy Fuels* **2018**, *32* (8), 8220−8229.

(17) Gauglitz, P. A.; Friedmann, F.; Kam, S. I.; Rossen, W. R. Foam generation in porous media. In *Proceedings of the SPE/DOE Improved Oil Recovery Conference*, Tulsa, OK, April 13−17, 2002; OnePetro, 2002; SPE-75177-MS. DOI: 10.2118/75177-MS

(18) Rossen, W. R.; Gauglitz, P. A. Percolation theory of creation and mobilization of foams in porous media. *AIChE J.* **1990**, *36* (8), 1176−1188.

(19) Yu, G.; Vincent-Bonnieu, S.; Rossen, W. R. Foam propagation at low superficial velocity: implications for long-distance foam propagation. *SPE Journal* **2020**, *25* (06), 3457−3471.

(20) Rossen, W. R. Theory of mobilization pressure gradient of flowing foams in porous media: I. *Incompressible foam. Journal of Colloid and Interface Science* **1990**, *136* (1), 1−16.

(21) Chang, S. H.; Owusu, L. A.; French, S. B.; Kovarik, F. S. The effect of microscopic heterogeneity on CO2-foam mobility: Part 2-mechanistic foam simulation. In *Proceedings of the SPE/DOE Improved Oil Recovery Conference*, Tulsa, OK, April 22−25, 1990; OnePetro, 1990; SPE-20191-MS. DOI: 10.2118/20191-MS

(22) M'barki, O.; Ma, K.; Mateen, K.; Ren, G.; Luo, H.; Neillo, V.; Bourdarot, G.; Morel, D.; Nguyen, Q. Experimental Investigation of Multiple Pore Vololumes Needed to Reach Steady-state Foam Flow in a Porous Media. In *Proceedings of IOR 2019−20th European Symposium on Improved Oil Recovery*, April 2019; European Association of Geoscientists & Engineers; Vol. *2019*, pp 1−17. DOI: 10.3997/2214-4609.201900148

(23) Myers, T. J.; Radke, C. J. Transient foam displacement in the presence of residual oil: experiment and simulation using a population-balance model. *Industrial & engineering chemistry research* **2000**, *39* (8), 2725−2741.

(24) Apaydin, O. G.; Kovscek, A. R. Surfactant concentration and end effects on foam flow in porous media. *Transport in porous media* **2001**, *43*, 511−536.

(25) Nguyen, Q. P.; Currie, P. K.; Zitha, P. L. Determination of foam induced fluid partitioning in porous media using X-ray computed tomography. In *Proceedings of the International Conference on Oilfield Chemistry*, Houston, TX, February 5−7, 2003; OnePetro, 2003; SPE-80245-MS. DOI: 10.2118/80245-MS

(26) Almajid, M. M.; Nazari, N.; Kovscek, A. R. Modeling steady-state foam flow: hysteresis and backward front movement. *Energy Fuels* **2019**, *33* (11), 11353−11363.

(27) AlYousef, Z.; Gizzatov, A.; AlMatouq, H.; Jian, G. Effect of Crude Oil on CO2−Foam Stability. In *Proceedings of the Offshore Technology Conference Asia*, Kuala Lumpur, Malaysia, November 2−6, 2020; OnePetro, 2020; OTC-30210-MS. DOI: 10.4043/30210-MS
(28) Beunat, V.; Pannacci, N.; Batot, G.; Gland, N.; Chevallier, E.; Cuenca, A. Study on the Impact of Core Wettability and Oil Saturation on the Rheological Behavior of CO2-Foams. In *Proceedings of the SPE Middle East Oil and Gas Show and Conference*, Manama, Bahrain, March 18−21, 2019; OnePetro, 2019; SPE-194963-MS. DOI: 10.2118/194963-MS
(29) Chen, H.; Elhag, A. S.; Chen, Y.; Noguera, J. A.; AlSumaiti, A. M.; Hirasaki, G. J.; Nguyen, Q. P.; Biswal, S. L.; Yang, S.; Johnston, K. P. Oil effect on CO2 foam stabilized by a switchable amine surfactant at high temperature and high salinity. *Fuel* **2018**, *227*, 247−255.
(30) Jian, G.; Zhang, L.; Da, C.; Puerto, M.; Johnston, K. P.; Biswal, S. L.; Hirasaki, G. J. Evaluating the transport behavior of CO2 foam in the presence of crude oil under high-temperature and high-salinity conditions for carbonate reservoirs. *Energy Fuels* **2019**, *33* (7), 6038−6047.
(31) Hosseini-Nasab, S. M.; Zitha, P. L. J. Chemical-foam Design as a Novel Approach Towards Immiscible Foam Flooding for Enhanced Oil Recovery. In *Proceedings of IOR 2017−19th European Symposium on Improved Oil Recovery*, April 2017; European Association of Geoscientists & Engineers, 2017; Vol. *2017*, pp 1−16. DOI: 10.3997/2214-4609.201702311
(32) Jian, G.; Fernandez, C. A.; Puerto, M.; Sarathi, R.; Bonneville, A.; Biswal, S. L. Advances and challenges in CO2 foam technologies for enhanced oil recovery in carbonate reservoirs. *J. Pet. Sci. Eng.* **2021**, *202*, 108447.
(33) Belhaj, A. F.; Elraies, K. A.; Mahmood, S. M.; Zulkifli, N. N.; Akbari, S.; Hussien, O. S. The effect of surfactant concentration, salinity, temperature, and pH on surfactant adsorption for chemical enhanced oil recovery: a review. *Journal of Petroleum Exploration and Production Technology* **2020**, *10*, 125−137.
(34) Amirmoshiri, M.; Zhang, L.; Puerto, M. C.; Tewari, R. D.; Bahrim, R. Z. B. K.; Farajzadeh, R.; Hirasaki, G. J.; Biswal, S. L. Role of wettability on the adsorption of an anionic surfactant on sandstone cores. *Langmuir* **2020**, *36* (36), 10725−10738.
(35) Heberling, F.; Trainor, T. P.; Lützenkirchen, J.; Eng, P.; Denecke, M. A.; Bosbach, D. Structure and reactivity of the calcite−water interface. *J. Colloid Interface Sci.* **2011**, *354* (2), 843−857.
(36) Song, J.; Zeng, Y.; Wang, L.; Duan, X.; Puerto, M.; Chapman, W. G.; Biswal, S. L.; Hirasaki, G. J. Surface complexation modeling of calcite zeta potential measurements in brines with mixed potential determining ions (Ca2+, CO32−, Mg2+, SO42−) for characterizing carbonate wettability. *J. Colloid Interface Sci.* **2017**, *506*, 169−179.
(37) Chen, Y.; Elhag, A. S.; Poon, B. M.; Cui, L.; Ma, K.; Liao, S. Y.; Reddy, P. P.; Worthen, A. J.; Hirasaki, G. J.; Nguyen, Q. P.; Biswal, S. L.; Johnston, K. P. Switchable nonionic to cationic ethoxylated amine surfactants for CO2 enhanced oil recovery in high-temperature, high-salinity carbonate reservoirs. *SPE J.* **2014**, *19* (02), 249−259.
(38) Cui, L.; Ma, K.; Abdala, A. A.; Lu, L. J.; Tanakov, I.; Biswal, S. L.; Hirasaki, G. J. Adsorption of a switchable cationic surfactant on natural carbonate minerals. *SPE Journal* **2015**, *20* (01), 70−78.
(39) Zhang, L.; Jian, G.; Puerto, M.; Wang, X.; Chen, Z.; Da, C.; Johnston, K.; Hirasaki, G.; Biswal, S. L. Crude Oil Recovery with Duomeen CTM-Stabilized Supercritical CO_2 Foams for HPHT and Ultrahigh-Salinity Carbonate Reservoirs. *Energy Fuels* **2020**, *34* (12), 15727−15735.
(40) Al Mahrouqi, D.; Vinogradov, J.; Jackson, M. D. Zeta potential of artificial and natural calcite in aqueous solution. *Advances in colloid and interface science* **2017**, *240*, 60−76.
(41) Li, S.; Jackson, M. D.; Agenet, N. Role of the calcite-water interface in wettability alteration during low salinity waterflooding. *Fuel* **2020**, *276*, 118097.
(42) Deposition no. PCT/FR2023/051334.
(43) Chen, X.; Da, C.; Hatchell, D. C.; Daigle, H.; Ordonez-Varela, J. R.; Blondeau, C.; Johnston, K. P. Ultra-stable CO2-in-water foam by generating switchable Janus nanoparticles in-situ. *J. Colloid Interface Sci.* **2023**, *630*, 828−843.
(44) Mannhardt, K.; Svorstøl, I. Surfactant concentration for foam formation and propagation in Snorre reservoir core. *J. Pet. Sci. Eng.* **2001**, *30* (2), 105−119.
(45) Lotfollahi, M.; Farajzadeh, R.; Delshad, M.; Varavei, A.; Rossen, W. R. Comparison of implicit-texture and population-balance foam models. In *Proceedings of the SPE EOR Conference at Oil and Gas West Asia*, Muscat, Oman, March 21−23, 2016; OnePetro, 2016; SPE-179808-MS. DOI: 10.2118/179808-MS
(46) Ma, K.; Ren, G.; Mateen, K.; Morel, D.; Cordelier, P. Modeling techniques for foam flow in porous media. *SPE Journal* **2015**, *20* (03), 453−470.
(47) Farajzadeh, R.; Lotfollahi, M.; Eftekhari, A. A.; Rossen, W. R.; Hirasaki, G. J. H. Effect of permeability on implicit-texture foam model parameters and the limiting capillary pressure. *Energy Fuels* **2015**, *29*, 3011−3018.
(48) Vavra, E.; Bai, C.; Puerto, M.; Ma, K.; Mateen, K.; Hirasaki, G. J.; Biswal, S. L. Effects of velocity on N2 and CO2 foam flow with in-situ capillary pressure measurements in a high-permeability homogeneous sandpack. *Sci. Rep.* **2023**, *13*, 10029.
(49) Ding, L.; Jouenne, S.; Gharbi, O.; Pal, M.; Bertin, H.; Rahman, M. A.; Economou, I. G.; Romero, C.; Guérillot, D. An experimental investigation of the foam enhanced oil recovery process for a dual porosity and heterogeneous carbonate reservoir under strongly oil-wet condition. *Fuel* **2022**, *313*, 122684.
(50) Blunt, M. J.; Bijeljic, B.; Dong, H.; Gharbi, O.; Iglauer, S.; Mostaghimi, P.; Paluszny, A.; Pentland, C. Pore-scale imaging and modelling. *Adv. Water Res.* **2013**, *51*, 197−216.
(51) Bijeljic, B.; Mostaghimi, P.; Blunt, M. J. Insights into non-Fickian solute transport in carbonates. *Water Resour. Res.* **2013**, *49* (5), 2714−2728.
(52) Jones, S. A.; Kahrobaei, S.; Van Wageningen, N.; Farajzadeh, R. CO2 Foam Behavior in Carbonate Rock: Effect of Surfactant Type and Concentration. *Ind. Eng. Chem. Res.* **2022**, *61* (32), 11977−11987.

https://doi.org/10.1021/acsomega.4c04137
ACS Omega 2024, 9, 37094−37104